RSC Advances

PAPER

View Article Online
View Journal | View Issue

Cite this: *RSC Adv.*, 2024, **14**, 11244

An examination of the effectiveness of the expired drug isoprinosine in preventing aluminum corrosion in alkaline solutions using both computational and experimental techniques†

S. M. Syam, *[a] Emad E. El-Katori,[b] Ahmed. A. Elhenawy, [cd] H. Nady[ef] and Salah Eid*[ae]

A now-expired medication called isoprinosine was examined in NaOH (0.50 M) solutions as a potential novel inhibitor of aluminum corrosion. The inhibitory effectiveness of the isoprinosine compounds was examined utilizing different electrochemical tests (open circuit potential OCP, potentiodynamic polarization and electrochemical impedance spectroscopy EIS), surface examination and quantum calculations. Increases in isoprinosine concentration were seen to increase the inhibitory efficacy. It was discovered that the inhibitory action, which results in the inhibition of charge and mass transfer and protects the aluminum against harmful ions, was brought on by isoprinosine molecules adhering to the aluminum surface. Additionally, the surface morphology of Al dissolved in a 0.50 M NaOH solution without and with the existence of an isoprinosine molecule was analyzed using SEM/EDX and AFM techniques. Utilizing the optimized geometric parameters of the ground state molecules, FMO simulations and additional studies were executed successfully utilizing the density functional theory (DFT/B3LYP/6-311++G(d,p)). Based on the expected energies for the molecular carriers of charge, HOMO and LUMO. Calculations are also done for the AIM charges, Fukui functions, AIM charges, and excitation energies. Furthermore, molecular dynamic was simulated to explore the corrosion inhibition efficiency and mechanism of inhibition. The computational results are in the same agreement with experimental results, showing that isoprinosine can inhibit the corrosion of aluminum in 0.5 M NaOH.

Received 6th January 2024
Accepted 29th March 2024

DOI: 10.1039/d4ra00158c

rsc.li/rsc-advances

1. Introduction

Aluminum is commonly utilized as a crucial structural element in a variety of industries due to its superior functional and cost benefits, including surface coatings, aeroplanes, and batteries.[1,2] Yet, corrosion affects it just like it does with other metals. When metallic structures are slowly harmed by chemical or electrochemical reactions, it is called corrosion. Many studies have been done on the corrosion of aluminum in various mediums.[3–9] One of the most dangerous media for aluminum corrosion is the alkaline medium.[10–15] To stop or mitigate these negative impacts, a variety of tactics must be employed. Utilizing inhibitors serves as one of the most successful strategies for avoiding corrosion, such as certain chemical compounds containing aromatic rings, heteroatoms, or π-electrons.[16–20] It is recognized that coordinate bonds are stronger and display significant inhibitory efficiency in heterocyclic organic compounds.

Due to their high cost and extreme toxicity to both humans and the environment, the inhibitors utilized can also carry considerable dangers. Outdated medication might be used to get around these drawbacks. Many medications are returned to their producers, where they will expire, costing the manufacturers money. Several of the components present in repurposed (or expired) medications can occasionally be recycled for a variety of purposes. These medications include a variety of organic chemicals that can be utilized as anti-corrosion agents to lessen metal dissolution.[21–44] One of the common drugs used to treat herpes is isoprinosine. It is possible to reuse isoprinosine, which is not sold, as an inhibitor for metal corrosion. Expired isoprinosine is inexpensive and safe for the environment and people to utilize.

[a]*Chemistry Department, Faculty of Science, Benha University, Benha, Egypt. E-mail: Samar.seyam@fsc.bu.edu.eg*
[b]*Chemistry Department, Faculty of Science, New Valley University, El-Kharga, 72511, Egypt*
[c]*Chemistry Department, Faculty of Science, Al-Azhar University, Nasr City, 11884, Cairo, Egypt*
[d]*Chemistry Department, Faculty of Science and Art, AlBaha University, Mukhwah, Al Bahah 65731, Saudi Arabia*
[e]*Chemistry Department, College of Science and Arts, Jouf University, Alqurayat, Saudi Arabia. E-mail: salaheed@ju.edu.sa*
[f]*Chemistry Department, Faculty of Science, Fayoum University, Fayoum, Egypt*

† Electronic supplementary information (ESI) available. See DOI: https://doi.org/10.1039/d4ra00158c

The purpose of this essay is to examine how the medication isoprinosine inhibits the dissolution of Al in a sodium hydroxide (0.50 M) solution. Potentiodynamic polarization (PP), AFM, SEM/EDX, electrochemical impedance spectroscopy [EIS] and Open circuit potential [OCP] techniques have all been employed in the inquiry. Additionally, DFT and MC modeling were used to research isoprinosine in order to understand the mechanism of corrosion prevention.

2. Experimental

2.1. Test solutions

Distilled water and sodium hydroxide of analytical grade were used to create each tested solution. Isoprinosine, inosine pranobex, also known as inosine acedoben dimepranol (INN) or methisoprinol, has been used as the new inhibitor. Under license from Newport Pharmaceuticals Limited, Dublin, Ireland, isoprinosine was manufactured in Abu-Sultan, Ismailia, Egypt, by Medical Union Pharmaceuticals. Isoprinosine is an antiviral drug that develops the body's immunity and presents as a solution. Each 5 ml of the medication includes 250 mg of Isoprinosine. A dilution was then used to generate the volume required to reach the target concentration. Isoprinosine has the chemical formula $C_{52}H_{78}N_{10}O_{17}$ and a molar mass of 1115.23 g mol^{-1}. The chemical structures of the three parts of inosine pranobex (inosine, acedoben and dimethylamino isopropanol with a ratio of 1 : 3 : 3) are shown in Fig. 1.

2.2. Electrochemical experiments

Utilizing a 3-electrode cell comprising a platinum (Pt) counter electrode, a saturated calomel electrode (SCE) as a reference electrode, and an aluminum metal working electrode (area = 0.8 cm^2), all electrochemical tests were carried out. Before usage, the Al electrode was polished with emery paper of various grades up to 2.5 × 10^3 grade, then washed with dimethyl ketone and distilled water. All tests were performed at 293 K. Every experiment was run at least twice in order to ensure repeatability. The electrochemistry software suite Versa Studio and Versa STAT 4 were linked to the electrochemical cell. For fifteen minutes, the Al electrode was submerged in the test solution prior to the experiment. At OCP, EIS experiment was performed using an AC voltage of 10^{-2} V with a sine wave frequency range of 10^{+5} : 0.1 Hz. We quantified the potentiodynamic polarization (PP) data by sweeping the electrode potential at a scan rate of 5 mV s^{-1} from −1900 to −1000 mV *vs.* SCE. Every assessment conducted for this investigation was conducted in a naturally aerated environment.

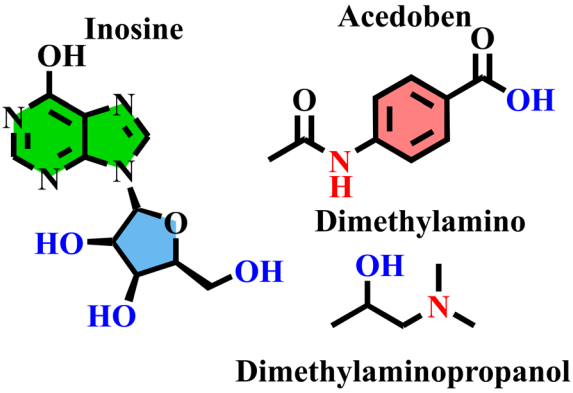

Fig. 1 Chemical structures of the three components of isoprinosine.

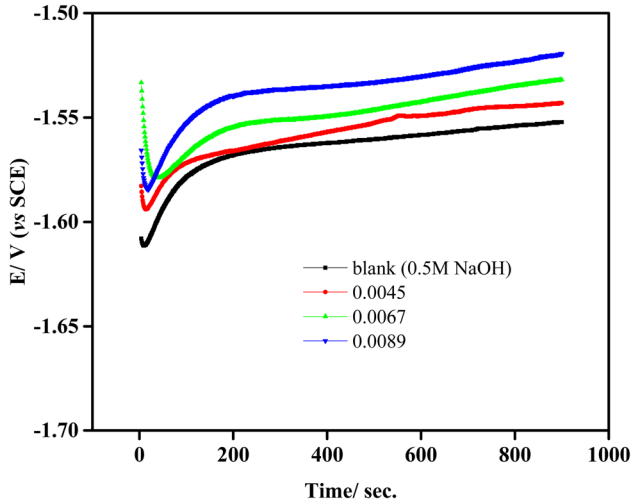

Fig. 2 Open-circuit potential of Al in 0.5 M NaOH in absence and presence of isoprinosine.

2.3. Surface measurements

The aluminum samples were scraped with various emery sheets up to a 2500 grade and then maintained in NaOH (0.50 M) with and without 0.011208 M of isoprinosine for 24 hours. The coupons were dehydrated, dried, and then inserted into the spectrometer following a distilled water cleaning. BED-C 10.0VKV, Jeol, a scanning electron microscopy (SEM) analysis observation tool, was utilized to examine the morphology of the Al surface. We performed the Atomic Force Microscopy (AFM) evaluation with the Nano Surf Flex AFM and C3000 controller.

2.4. Molecular modeling studies

A program named Materials Studio (developed by Accelrys Inc.) was used to do all of the quantum chemistry calculations using density functional theory (DFT) with free spin.[45] For DFT simulation, the generalized gradient approximation (GGA) of the Becke3-Lee-Yang-parr (B3LYP) level is used in the double-numeric basis set (DNP 4.4).[46] In addition to other molecular properties, including HOMO–LUMO, MEP & Fukui functions, the ideal structure also carried out the geometrical parameters. The electron localization function and the topological parameters were determined using the Atoms in Molecule (AIM) theory and Multiwfn software.

2.5. Molecular dynamic simulations

Molecular Dynamics (MD) simulation is used by the Adsorption Locator module in Materials Studio to simulate the attraction of

isoprinosines over the Al metal surface. To simulate the process of adsorption, the Al (1 1 0) plane's most stable surface was used. The simulation box for this plane measures (22.90 Å × 57.26 Å × 26.68 Å). For a vacuum layer, the box consists of an aluminum slab with a 15.00 Å. The connection between the total energy of the crystal when mixed with the isoprinosine "E_{total}" and the specific energy for the isoprinosine "E_{inh}" and the Al surface was used to indicate the interaction energy between Al and the isoprinosine "$E_{adsorption}$". Eqn (1) is designed to represent this relationship.

$$\text{“}E_{adsorption} = E_{total}\,(E_{Al} + E_{inhibitor})\text{”} \quad (1)$$

where E_{total} is the system total energy, E_{Al} the Al slab energy, and $E_{inhibitor}$ is the energy of inhibitor molecule. As an adsorption energy's negative sign value, the binding energy was determined.

3. Results and discussion

3.1. Open circuit potential (OCP)

The open circuit potential (OCP) *vs.* time graphs for aluminum in 0.5 M NaOH are shown in Fig. 2 in both the presence and absence of various amounts of isoprinosine. When aluminum is exposed to corrosive medium, OCP declines rapidly, which may be caused by the quick dissolution of the thin Al_2O_3 layer that has developed on the metal electrode, according to the exhaustive examination of the OCP *vs.* time curves.[47,48] Also, isoprinosine shifts the steady-state potential in an increased positive direction. This behavior is connected to the byproducts of the corrosion reaction that isoprinosine adsorbs and/or deposits on the aluminum surface, which may control and slow down the dissolution of aluminum. Furthermore, the features differ noticeably between the samples in the existence of several concentrations of isoprinosine and the uninhibited specimen. The samples' OCP *vs.* time curve was virtually straight at 15 minutes, indicating the accomplishment of steady-state potential.[49,50]

3.2. Potentiodynamic polarization (PP)

Aluminum PP curves in NaOH (0.50 M) solutions, both untreated and with varying amounts of isoprinosine, are shown in Fig. 3. The required electrochemical parameters are shown in Table 1 and include the percentage of inhibitory efficacy (% I. E. P), surface coverage (θ), corrosion current (i_{corr}), cathodic and anodic Tafel slopes (β_a and β_c) and corrosion potential (E_{corr}). With a view to computing the (% I. E. P) and surface coverage (θ), the following eqn (2) and (3) were used:[50–54]

$$\%\text{I. E. P} = \left(1 - \frac{i_{iso}}{i_{NaOH}}\right) \times 100 \quad (2)$$

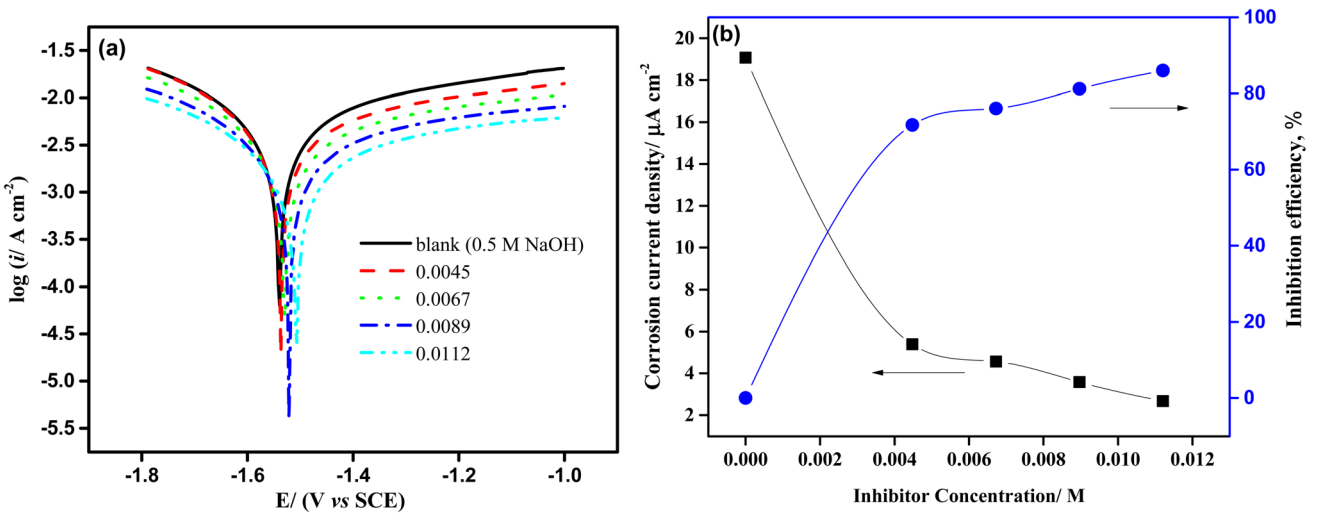

Fig. 3 (a) Potentiodynamic polarization graphs of aluminum electrode in 0.50 M NaOH solution containing different amounts of isoprinosine. (b) The effect of increasing concentration of isoprinosine on the current density and the inhibition efficiency.

Table 1 Polarization parameters of aluminum electrode in NaOH (0.50 M) solutions free and containing diverse concentrations of isoprinosine at 293 K

Inh. conc.	E_{corr}/mV$_{(SCE)}$	i_{corr}/mA cm^{-2}	β_a/mV dec^{-1}	$-\beta_c$/mV dec^{-1}	θ	% I. E. P
0	−1540	19.064	205.6	653.1	—	—
0.0045	−1532	5.39	748.3	334.2	0.7177	71.73
0.0067	−1528	4.56	897.6	335.5	0.7608	76.08
0.0089	−1519	3.58	843.1	360.8	0.8122	81.22
0.0112	−1511	2.67	835.9	290.2	0.8599	85.99

Table 2 Comparison of the inhibitory effectiveness of several expired drugs used for aluminum corrosion in various environments

Inhibitor	Concentration	Metal	Medium	Inhibition efficiency	References
Linezolid	250 mg L^{-1}	Al	1 M NaCl	71.00%	34
Norfloxacin	500 mg L^{-1}	Al	1 M NaCl	62.30%	34
Thiamine or vitamin B1	250 mg L^{-1}	Al	0.5 M H_2SO_4	91.14	36
Riboflavin or vitamin B2	250 mg L^{-1}	Al	0.5 M H_2SO_4	92.40	36
Voltaren	125 ppm	Al	1 M HCl	91.70%	40
Moxafloxacin	400 ppm	Al	1 M H_2SO_4	86.17%	41
Betnesol	400 ppm	Al	1 M H_2SO_4	95.40%	41
Ceftriaxone	300 ppm	Al	1 M NaOH	78.40%	42
Ceftazidime	300 ppm	Al	1 M NaOH	59.50%	42
Sildenafil drug	5×10^{-4} M	6063 aluminum alloy	1 M NaOH	90.59	43
Dapoxetine drug	5×10^{-4} M	6063 aluminum alloy	1 M NaOH	92.63	43
Theophylline	2.5%	7075 aluminium alloy	1 M NaOH	91.00	44
Isoprinosine	0.0112 M	Al	0.5 M NaOH	85.99%	This work

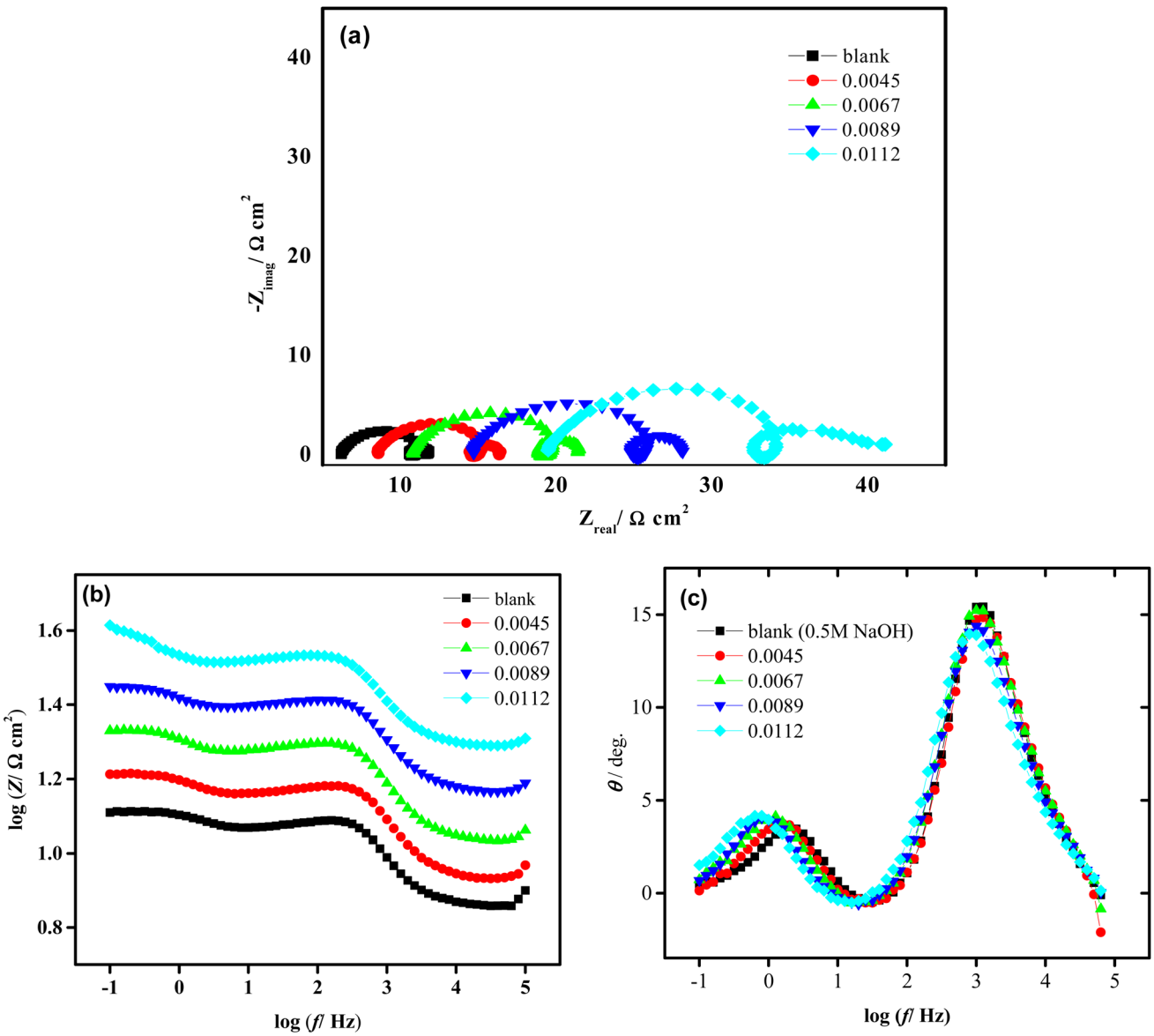

Fig. 4 Nyquist (a) and bode (b and c) plots of Al after electrode immersion in 0.5 M NaOH in absence and presence of isoprinosine inhibitor at 293 K.

$$\theta = \left(1 - \frac{i_{iso}}{i_{NaOH}}\right) \quad (3)$$

where i_{NaOH} and i_{iso} are the corrosion current density of the aluminum electrode in lack of and existence of isoprinosine, respectively. Fig. 3 shows that as isoprinosine concentration raised the corrosion current density shifted to lower values, causing a decrease in the rate of corrosion and an increase in inhibition efficiency. Table 1's analysis illustrates that as isoprinosine amounts is raised, the value of (i_{corr}) diminishes and the inhibitory activity rises to reach its maximum value, 85.99% at 0.0112 M. This output shows how the isoprinosine prevents aluminum in NaOH (0.50 M) solution from dissolution. Additionally, there is no obvious change in E_{corr} values; more so, the anodic and cathodic Tafel constants were significantly altered by the addition of increasing isoprinosine concentrations, which points to a mixed adsorption mechanism.[18] The experimental findings of this study are presented in Table 2 with those of other studies using aluminum corrosion inhibitors in various mediums. The dynamic polarization test results suggest that the protective layer formed by the isoprinosine components on aluminum surface in alkaline media has a strong anti-corrosion performance.

3.3. EIS measurements

Electrochemical impedance spectroscopy (EIS), is a highly effective method for examining complicated electrochemical systems. Fig. 4 displays aluminum EIS diagrams in both the lack and the existence of various Isoprinosine amounts. Additionally, this figure depicts depressed capacitive semicircles in the higher and lower frequency bands, separated by a low-frequency inductive loop.[12] Adsorbed intermediates were found on the aluminum surface throughout the dissolving process, which provided evidence for the inductive loop at medium frequencies.[30,55,56] Previously, it was thought that the capacitive semicircle at higher frequencies was caused by the relaxation of adsorbed species as OH^- or due to the $Al–Al^+$ redox reaction, which was also thought to be the rate-determining stage in the charge transfer process.[12,57–59] Consequently, the resistance for charge transfer between $Al–Al^+$ and the resistance indicated by the intercepts of the first capacitive semicircle with the real axis are equivalent. Moreover, the quick redox reaction between the Al^+ and Al^{3+} could be the cause of the second capacitive semicircle.[60,61] As the concentration of isoprinosine rises, it can be seen that the semicircle's diameter grows. This extend in capacitive semicircles demonstrates that the attraction of isoprinosine to the Al surface, which leads to greater resistance and a slower rate of corrosion, is what gives birth to their inhibitory action. The cell under study and its reaction mechanism must be understood in order to fit an EIS model to experimental results. In order to examine the impedance spectra of aluminum in caustic soda solutions, the analogous circuit presented in Fig. S1† was employed. In Table 3, the fitted findings for various isoprinosine concentrations are presented. Inspection of Table 3 demonstrates that inhibited systems exhibit higher R_{ct} values than uninhibited systems.[62] C_{dl} may decrease in inhibited systems when isoprinosine molecules replace high-dielectric water with lower-dielectric isoprinosine molecules, suggesting that the isoprinosine molecules bind to the metal/electrolyte interface and cause a decline in the local dielectric constant.[63]

3.4. Surface morphology

By analyzing the geometry of the surface, the sharpness of the corrosion assault may be ascertained. Aluminum specimens were observed using SEM/EDX after being dipped in 0.5 M NaOH, lacking and possessing 0.011208 M of isoprinosine, as shown in Fig. 5 and 6. Aluminum coupons in 0.5 M NaOH only showed a significantly deformed surface, as predicted by the SEM results, which detailed their morphological characteristics. Conversely, the aluminum surface appears to have fewer scratches and is finer (as shown in Fig. 6) in a 0.5 M NaOH solution with isoprinosine.[64–66]

Atomic or near-atomic resolution AFM surface topography images may be utilized to examine a coupon's surface roughness. The aluminum surface's AFM morphologies in NaOH (0.5 M) solutions are depicted in Fig. 7 in both the presence and lack of the isoprinosine inhibitor. As illustrated in Fig. 7, the aluminum surface's root mean square and average roughness in 0.5 M NaOH are greater than those of the aluminum sample with isoprinosine present. These results show that isoprinosine molecules have been attracted to the aluminum surface, successfully creating a safeguarding layer that defends the surface of aluminum from caustic soda.[23]

3.5. Adsorption isotherm

The interpretation of isoprinosine adsorption demeanor on the aluminum surface is made possible by locating a suitable isotherm. The exploratory data from PP measurements were fitted using Langumir, Freundlich, Temkin and Flory–Huggins

Table 3 Electrochemical parameters calculated from EIS measurements on aluminum electrode in NaOH (0.50 M) solutions free and containing diverse concentrations of isoprinosine at 293 K

Inh. conc.	R_s (Ω)	R_{ct1} (Ω cm^2)	CPE	R_{ct2} (Ω cm^2)	C_{dl}	R_L (Ω cm^2)	L	R_{ct3} (Ω cm^2)	C_f	Chi-squared χ^2	R_T (Ω cm^2)	% I. E. P
0	7.4	3.8	3.2×10^{-5}	0.517	8.5×10^{-5}	0.6	0.002439	1.4	0.06369	0.0009936	6.34	—
0.0067	10.9	4.9	1.5×10^{-5}	2.9	2.7×10^{-5}	1.2	0.006234	2.9	0.05321	0.0003527	11.9	46.7
0.0089	14.8	0.1	3.8×10^{-5}	9.9	4.1×10^{-6}	1.9	0.006668	3.5	0.05725	0.0002367	15.4	58.8
0.0112	19.6	0.1	3.7×10^{-5}	13.2	7.2×10^{-11}	0.22	0.01031	6.7	0.04721	0.0002816	20.2	68.7

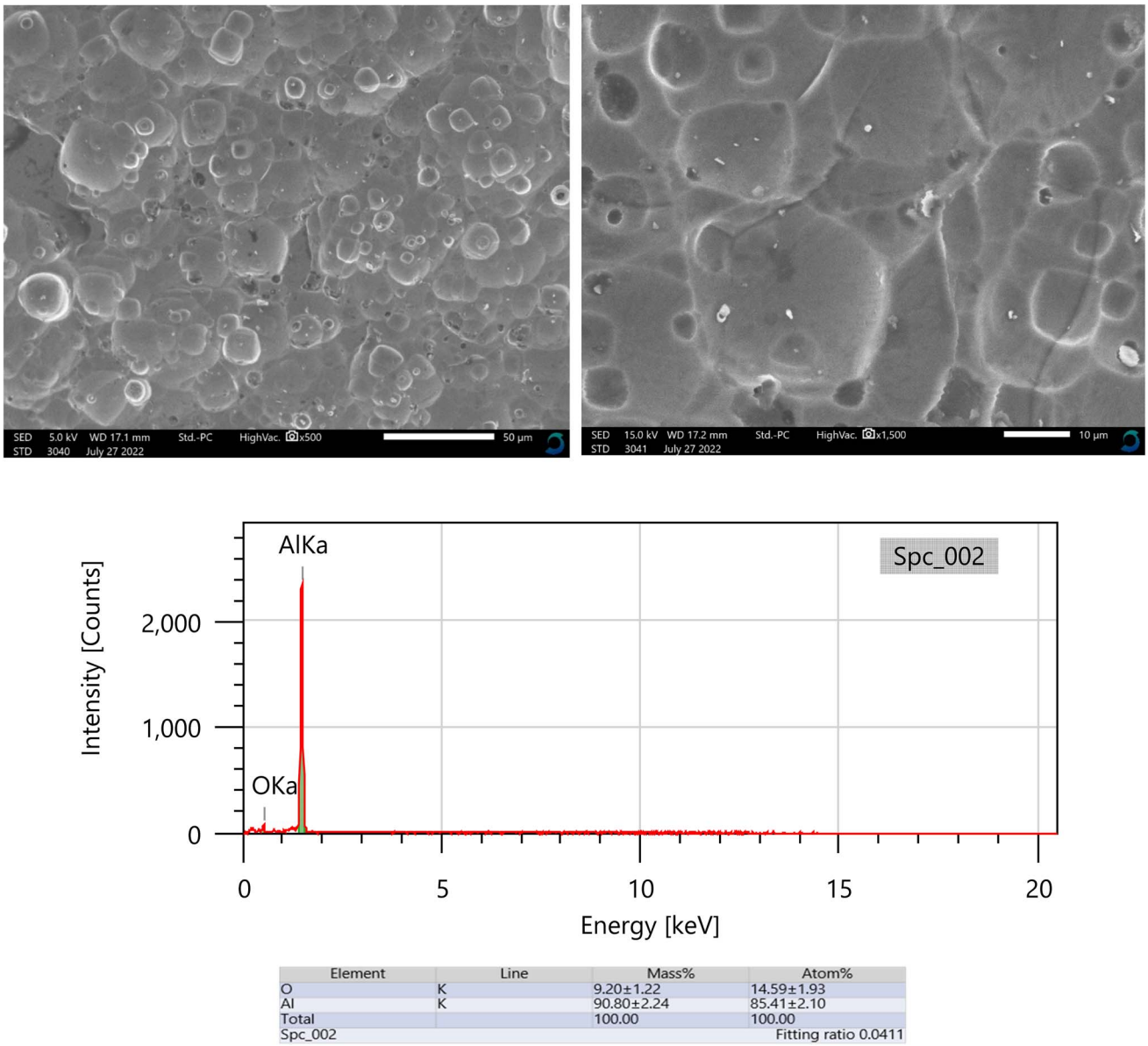

Fig. 5 SEM/EDX for Al after immersion 0.5 M NaOH in the absence of isoprinosine.

isotherm relations.[67] Our findings, as shown in Fig. S2,† meet the Langmuir isotherm eqn (4):[68]

$$\frac{C}{\theta} = \frac{1}{k} + C, \quad (4)$$

where K and C symbolize the equilibrium constant for the process of adsorption and the isoprinosine concentration, respectively. Fig. S2† displays a graph of $\frac{C}{\theta}$ *vs.* C. The equilibrium constant for adsorption, K, and the standard free energy of adsorption, ΔG°_{ads}, are related by the eqn (5):[69]

$$K = \frac{1}{55.5}\exp\left(\frac{-\Delta G^{\circ}}{RT}\right) \quad (5)$$

where the number 55.5 symbolizes the water molar concentration and the letters R and T symbolize the ideal gas constant and the absolute temperature, respectively. The standard adsorption free energy is equal to −25.1 kJ mol^{-1}, and the equilibrium constant is equal to 526. The negative sign of "ΔG°_{ads}" denotes the adsorption of isoprinosine on the Al surface occurring spontaneously.[69]

3.6. Molecular modeling studies

3.6.1. Isoprinosine frontier orbital analysis. Conceptual DFT is a useful tool to recognize the reactivity of chemical processes. It involves the calculation of reactivity indices, such as the LRI and the GRI, which measure the local and global tendency of a molecule to react. These indices can help compare the reactivity of different molecules or reactions, and they can also predict the most favorable reaction pathways and mechanisms. This can help optimize synthetic strategies and design

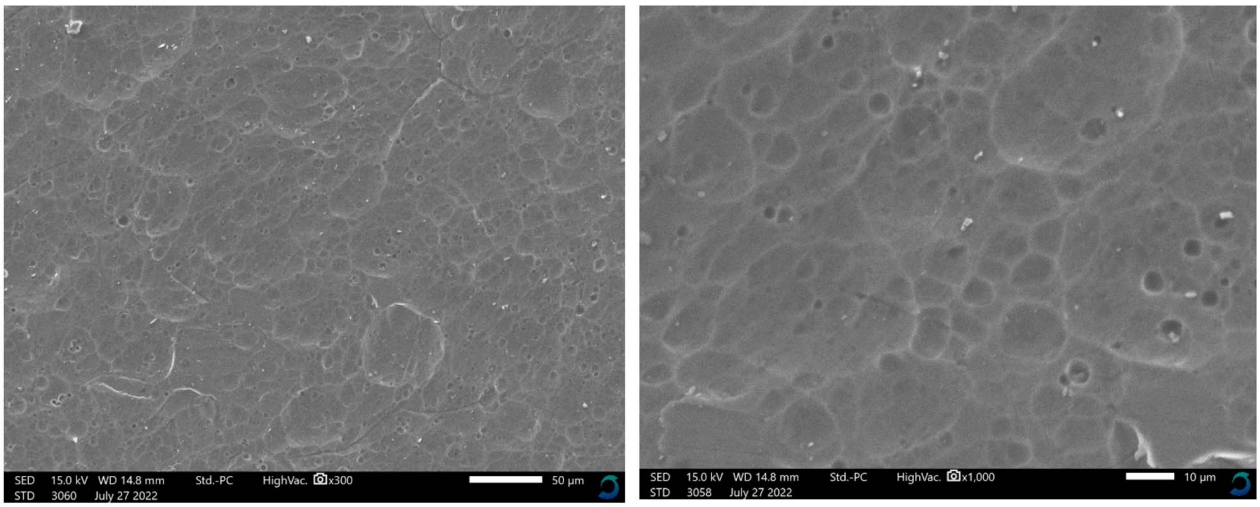

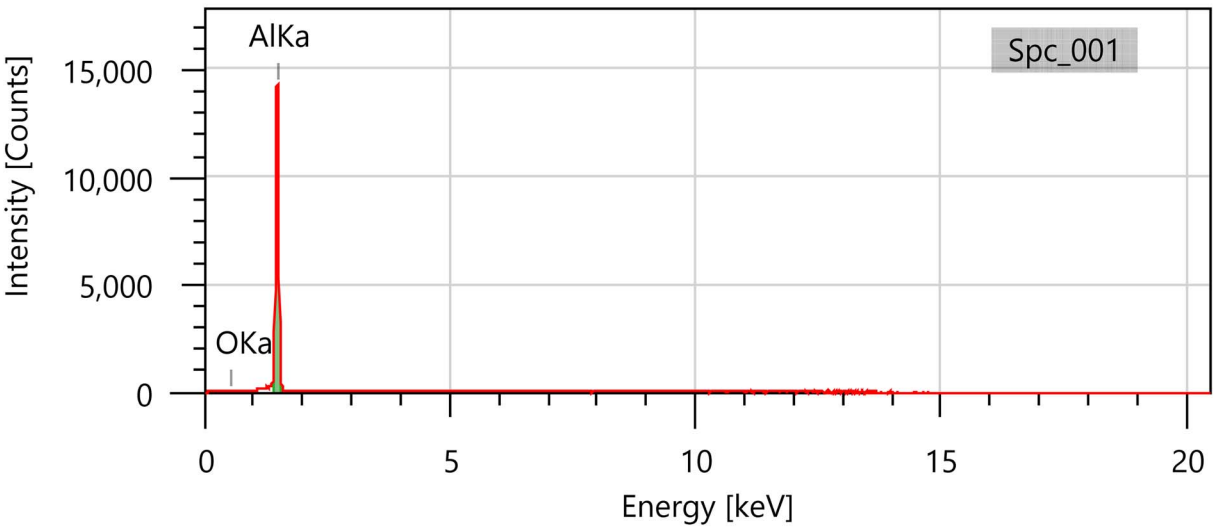

Element	Line	Mass%	Atom%
O	K	1.10±0.19	1.83±0.32
Al	K	98.90±0.99	98.17±0.98
Total		100.00	100.00
Spc_002			Fitting ratio 0.0094

Fig. 6 SEM/EDX for Al after immersion 0.5 M NaOH in the presence of 0.01 M of isoprinosine inhibitor.

new reactions. The global indices used in this study are electronic chemical potential φ, global electrophilicity ω, chemical hardness η and global nucleophilicity N, as well as the maximum number of electrons transferred (ΔN_{max}) for isoprinosine (see Table 4). These indices indicate the stability and reactivity of the interaction between the LUMO of the surface and the HOMO of isoprinosine. The adsorption of isoprinosine on Al surface was studied by calculating the ΔG values for different components of the drug. The results showed that inosine had the lowest ΔG value (3.6 eV), followed by Acedoben (4.7 eV) and dimethylaminopropanol (5.3 eV). The ΔG values increased with the hardness of the electrophiles and the softness of the nucleophiles in the drug components. As a result, nucleophiles and electrophiles have been defined using soft and hard terminology that are directly related to ΔG. An effective inhibitor molecule in basic medium is anticipated for the small ΔG, due to its high softness characteristics. On the other hand, hard molecules have high ΔG and are ineffective inhibitors of corrosion.[70]

The phrase (μ) "electron donating potency" refers to how many electrons the inhibitor is capable of transferring from itself as a donor to the metal as an acceptor molecule.[71] isoprinosine's inhibitory activity increases with its ability to contribute more electrons. Therefore, higher electron donating potencies are ordered as inosine, dimethylaminopropanol, and acedoben. On the other hand, the lower the electron accepting ability (ω) of the isoprinosine on the metal surface, the lower its inhibition efficiency. Among the inhibitors, dimethylaminopropanol has the lowest electron accepting ability and, hence, the lowest inhibition effect. The work function of aluminum is

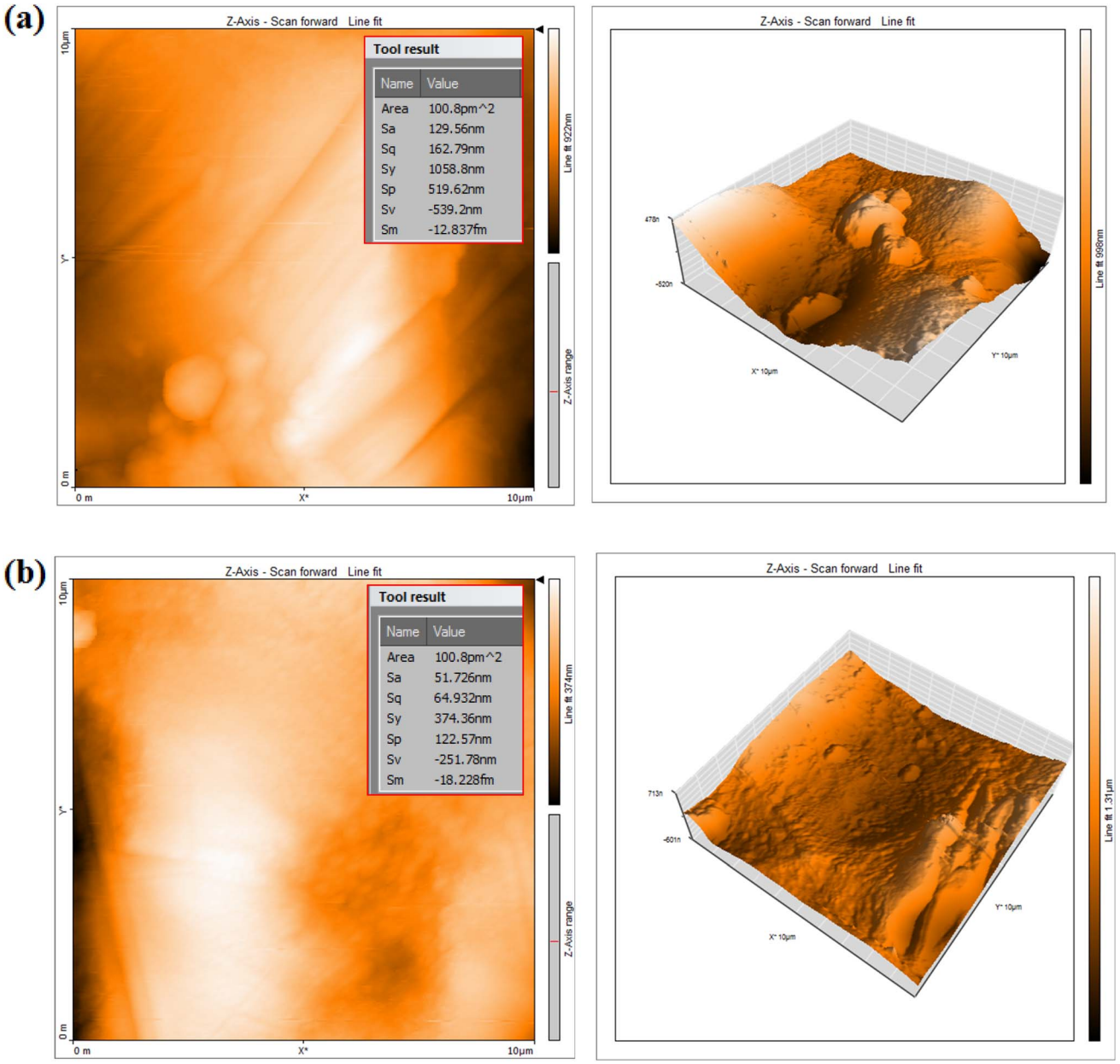

Fig. 7 AFM for Al after immersion 0.5 M NaOH in the absence (a) and presence (b) of 0.0112 M of isoprinosine inhibitor.

Table 4 Isoprinosine electronic chemical potential φ, chemical hardness η, global electrophilicity ω and global nucleophilicity μ

Species	HOMO	LUMO	$\Delta\varepsilon$	η	S	φ	μ	ω	ΔN_{max}	ΔN_{BD}
Dimethylaminopropanol	−6.201	−0.851	5.349	2.674	0.373	3.526	−1.245	0.807	0.146	−1.047
Acedoben	−5.983	−1.241	4.742	2.371	0.421	3.612	−1.9325	0.583	0.288	−1.2187
Inosine	−5.461	−1.851	3.609	1.807	0.554	3.656	−2.125	0.620	0.188	−1.277

4.28 eV.[72] The work function is the amount of energy necessary to transfer an electron from a solid to a location outside the solid's surface. Furthermore, the maximum number of electrons transferred (ΔN_{max}) value was obtained using eqn (6):

$$\Delta N = \frac{(\phi_{Al} - \phi_{inh})}{(\eta_{Al} + \eta_{inh})} \quad (6)$$

where ϕ_{Al} and ϕ_{inh} are the work functions of the metal and the isoprinosine, respectively, η_{inh} is the hardness of the isoprinosine, and η_{Al} was assumed to be zero since the ionization potential of the metal is equal to its electron affinity. A positive ΔN value indicates that the isoprinosine donates electrons to the surface of aluminum, whereas a negative ΔN value implies that the isoprinosine accepts electrons from the surface of

aluminum. The dipole moment (D) of the isoprinosine molecule reflects its ability to polarize the electric double layer and enhance its adsorption on the metal surface. A higher D value implies better corrosion inhibition performance. The computed values of ΔN and D are shown in Table 4. Table 4 showed, highest ΔN value for dimethylaminopropanol than other components. That means that it acts as an electron donor to the Al surface. The return of donating electrons from metal to isoprinosine is referred to as "$\Delta E_{\text{Back-donation}}$", which determine binding interaction of isoprinosine with metal surface. isoprinosine molecule has high $\Delta E_{\text{Back-donation}}$, can have strong penetration ability, and increases inhibition efficiency. The negative values of ($\Delta E_{\text{Back-donation}}$) suggested that the electron follows from metal to isoprinosine to be energetically favorable. This suggests that isoprinosine has a strong polarizing effect on the electric double layer and forms a stable adsorption layer on the metal surface. Thus, based on these theoretical calculations, it can be considered an effective corrosion inhibitor for Al.

3.6.2. HOMO–LUMO and MEP (electrostatic potential map). The highest occupied molecular orbital (HOMO) and lowest unoccupied molecular orbital (LUMO) play a crucial role in determining the chemical behavior of a molecule. HOMO and LUMO are localized on the overall molecular skelton dimethylaminopropanol and acedoben. Consequently, these orbitals are distributed around the purine ring of Inosine (Fig. 8). The plot of HOMO shows that the positive and negative regions are spread all over the molecule. The detecting corrosion efficiency is explained by the charge transfer interaction between the molecules and the Al surface. MEP is a signature for the polarization of the outer electrons and the distribution of those electrons in relation to the molecular environment's reactivity and ability to interact with H-atoms. Additionally, it provides complete information on electrophilic and nucleophilic chemical locations. As a result, we can graphically determine the statistical polarity, through variations in color in Fig. 8, which served to distinguish the polar ("−" charge as red color) and nonpolar ("+" charge as blue color) molecular zones. It was found that the green area's potential fell halfway between the dual red and blue. Red, yellow, blue, and green emerge in ascending order when the color distribution on MEP changes (Fig. 8). The electron distribution revealed that, depending on their size and structure, isoprinosine molecules may bind to metal ions. Fig. 8 demonstrated how the oxygen in dimethylaminopropanol, C=O, acedoben, and inosine, as well as their OH groups, increased the electrophilicity impact. Isoprinosine's nucleophilicity was activated by the blue highlight that covered the substance's hydrogen atoms.

3.6.3. Topology estimation. Fig. 8 shows the topological study of the atoms in the molecule, which was used to learn more about the type of intramolecular interactions in the

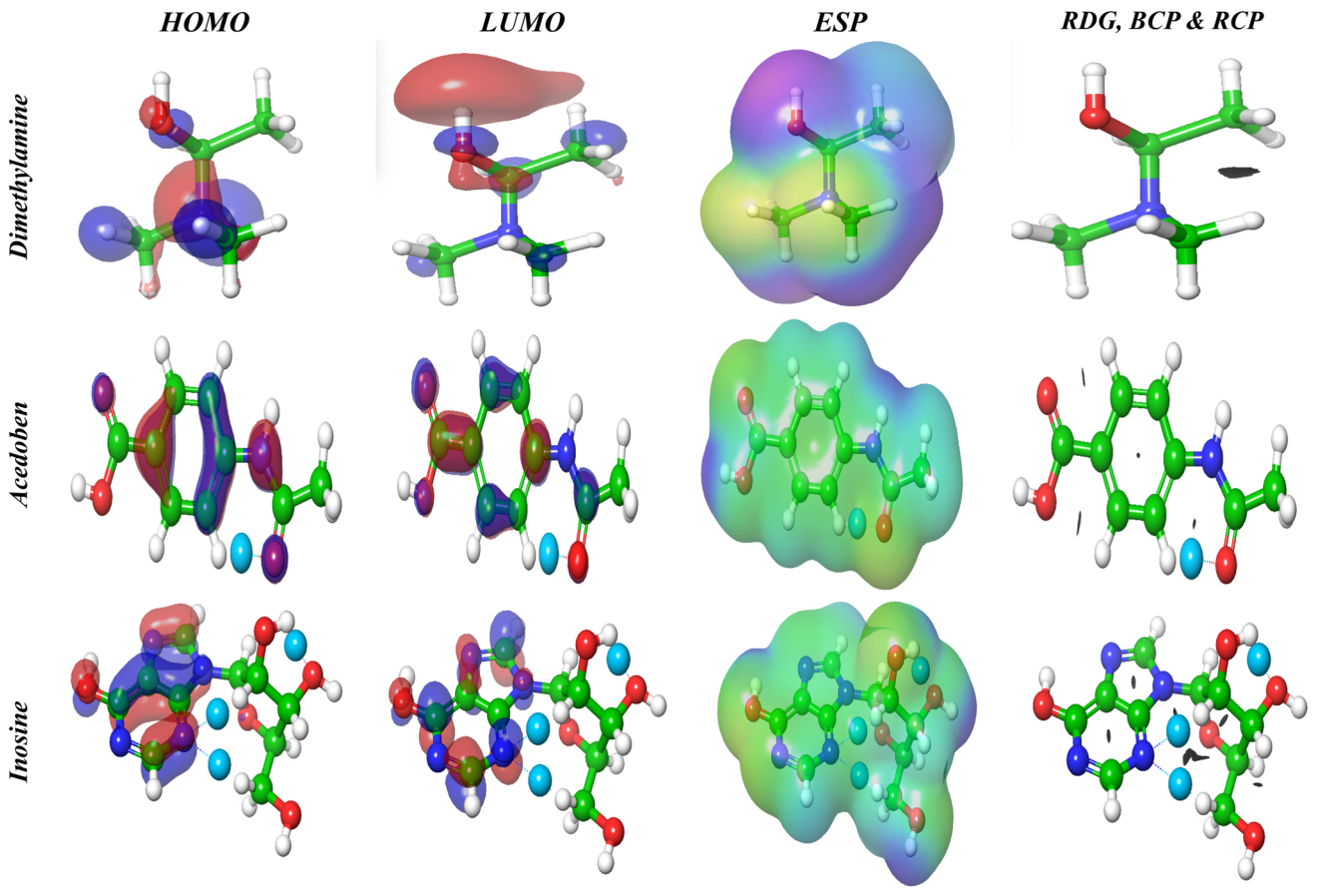

Fig. 8 HOMO, LUMO and ESP at DFT; BCP, RCP and RDG using AIM theory.

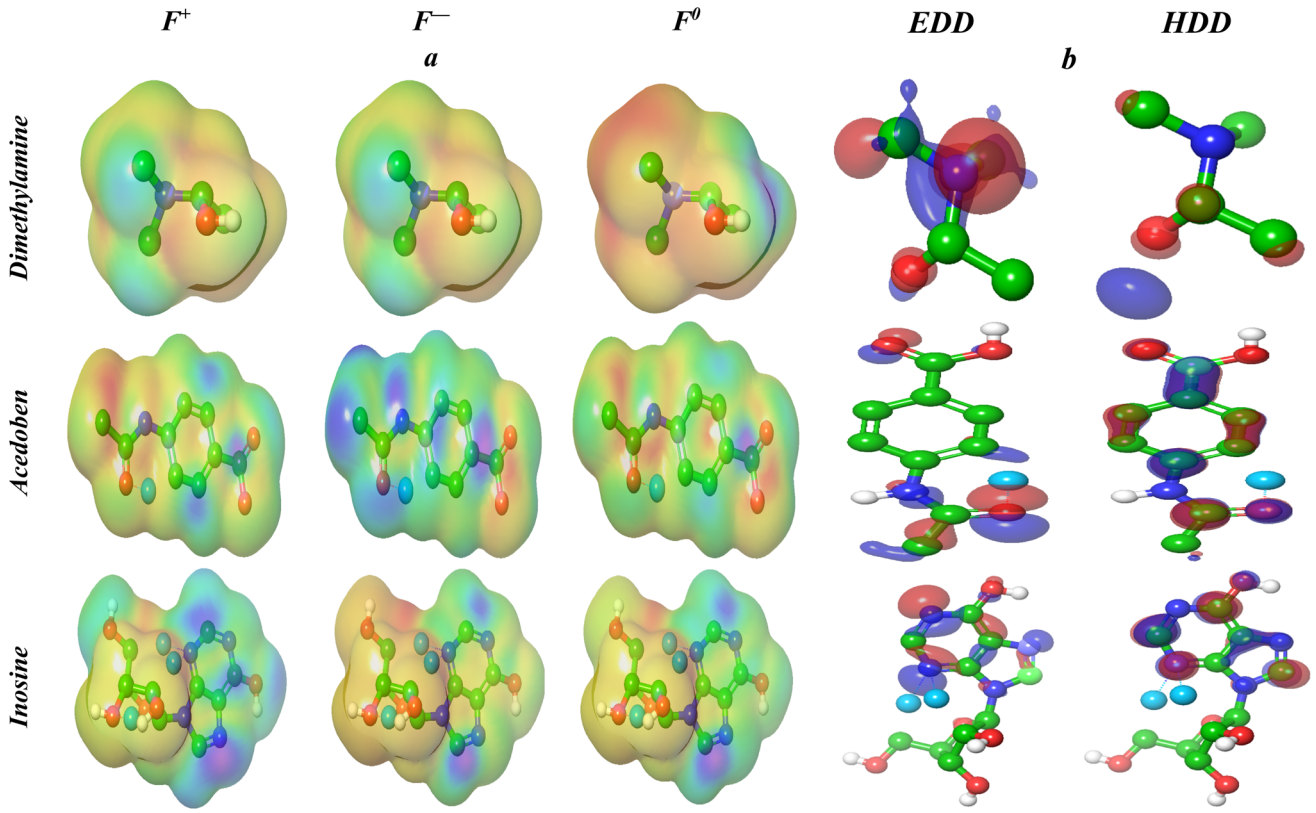

Fig. 9 (a) 3D-representation of the R_k molecular map of reactivity of cation, anion and neutral; for compounds for Isoprinosine, $R_k > 0$, correspond to electrophilic centers, while $R_k < 0$, corresponds to nucleophilic centers; (b) EDD and HDD profiles for the excited state.

isoprinosine component. The existence of a bond critical path (BCP), which Atoms in Molecule (AIM) analysis interprets as blue dots, assures the bond between the atoms. Fig. 8 displays BCP formed in acedoben at ($O_1\cdots H_{18}$) and inosine ($O_{19}\cdots H_{30}$, $N_{14}\cdots H_{22}$ and $N_{14}\cdots H_{26}$), respectively. While the ring critical path (RCP; blue surface) formed in the benzene ring of acedoben and the purine ring of Inosine. The nature of bonds can be described by the total electron density $p_{(r)}$ and its Laplacian ($\nabla^2 p_{(r)}$). The total electron density can be written as shown in eqn (7):

$$\frac{1}{4}\nabla^2 p_{(r)} = G(r) + \gamma\{r\} \quad (7)$$

where $G(r)$ and $V(r)$ are the kinetic and potential energy densities at critical points, respectively. The bond's strength can be inferred from the signs of $\nabla^2 p_{(r)}$ and $G(r_{BCP})+V(r_{BCP})$. If both are positive, the bond is weak. The ratio $G(r_{BCP})/V(r_{BCP})$ suggests that the hydrogen bond is non-covalent.[73]

3.6.4. Non-covalent interactions (NCI). A variety of interactions, such as electrostatic, covalent, and non-covalent ones, have an impact on the structural characteristics of the isoprinosine's constituents. Non-Covalent Interactions (NCI) may be found using Reduced Density Gradient (RDG) analysis, and their strength is shown as dashed lines. We applied the RMSD score to generate several structural poses. The sign and magnitude of this score indicate the type and strength of the interactions between the molecules. Hydrogen bonds have big negative values, repulsive interactions have large positive values, and weak van der Waals interactions have values close to zero. The sign (λ_2) values also reveal the nature of the bonding. Fig. 8 illustrates molecules with weak van der Waals contacts (green isosurfaces) in acedoben and inosine, respectively, as well as hydrogen bonding between $N_{14}\cdots H_{26}$ and $O_{19}\cdots H_{30}$ in inosine (blue isosurface sign $(\lambda_2)\rho$ value almost (-0.010).[74]

3.6.5. Electron excitation analysis based on the electron and hole density distribution. The idea of multi-molecular orbital excitation is provided by the distribution of electrons and total density, and this excitation state's characteristics are made obvious for receptors and the receptor anions that correspond to them. The characteristics and electrical structure of the isoprinosine molecule may be understood by examining the electron and overall density distribution. One way to study how molecules interact and bind with each other in receptor-ligand and metal–ligand systems is to use the data from the electronic transitions. These transitions involve the movement of an electron from a lower to a higher energy molecular orbital (MO) within the molecule. The higher energy MO represents the state where the electron is shared between two parts of the molecule in a single electron transfer process. The ground state MO and the excited state MO have different characteristics, which can be seen by comparing the electron density distribution maps of photo-excited states. The energy level of the excited state, the kind and location of the excited electrons, and the extent of electron delocalization are all indicated by these maps,

Table 5 Binding energy of MD simulation in kcal mol^{-1} for isoprinosine against Al surface

	Dimethylamino propanol	Acedoben	Inosine
Total energy	0.551	55.576	11.167
Adsorption energy	−392.440	−21978.4	−33805.34
Rigid adsorption energy	−3.4205	−7.863	−7.170
Deformation energy	−389.019	−21970.54	−33798.17
dEad/dNi	−392.440	−21998.4	−33825.34

which also depict how the electrons are distributed spatially within the molecule. The density distribution maps of electrons ($\rho_{ele(r)}$) and holes ($\rho_{hole(r)}$) can be utilized to examine the electron and overall density distribution (EDD and HDD) of a molecule. These maps are calculated by the following equations, which show the transition of an electron from an occupied MO(i) to a virtual MO (j) using the molecular orbital (MO) wave function (Φ) and the configuration coefficient (w):[30] $\rho_{ele(r)} = \Sigma i w_i \Phi_{i(r)}{}^2 \Phi_{j(r)}{}^2$, $\rho_{hole(r)} = \Sigma i w_i \Phi$. The EDD map in Fig. 9 reveals a thicker surface on the N atom of dimethylaminopropanol, the O atom of C=O in acedoben, and the N-atom of pyrimidine in inosine, suggesting that these areas have a greater electron density. Conversely, the HDD map displays a denser surface on the O, phenyl, and purine rings for dimethylaminopropanol, acedoben, and inosine, respectively, signifying a larger hole density.

3.6.6. Local DFT reactivity indices of reactants. The species' most electrophilic and nucleophilic sites can be determined by looking up the local reactivity difference index (R_k) for a particular reaction. By converting the spin electron density from nucleophile to electrophile, GEDT (Global Electron Density Transfer) processes provide nucleophilic/electrophilic Parr functions that can be used to assess the local reactivity inside polar systems. By defining the local reactivity of the species involved in a reaction, the R_k and GEDT techniques can offer insights into the system's overall reactivity. The R_k molecular map of reactivity (RMMR) for the chosen cation, anion, and neutral of dimethylaminopropanol, acedoben, and inosine is illustrated in three dimensions in Fig. 9. The illustration also displays the electrophilic $p_k{}^+$ Parr function and the nucleophilic $p_k{}^-$ function. The RMMR and Parr functions help identify the most electrophilic and nucleophilic centers of the molecule, which reveal important information about the system's reactivity. Based on the R_k values given, the $N(CH_3)_2$, phenyl, and pyrimidine rings are the electrophilic activation centers for dimethylaminopropanol, acedoben, and inosine, respectively.

3.6.7. Molecular dynamic simulations. An analysis of the isoprinosine-Al surface interaction using molecular dynamic (MD) modeling was carried out (Fig. S3†). Before beginning the adsorption procedure, the optimization geometry for the isoprinosine components was carried out. Using an adsorption locator model, the ideal adsorption location for an inhibitor molecule to adhere to an aluminum surface was found. The perfect adsorption site's lowest computed energies (in kcal mol^{-1}) are shown in Table 5. These energies include the total energy (the energy of the substrate-adsorbate system), the rigid adsorption energy (the energy of the inhibitor components that do not change their shape when adsorbed on the aluminum), the deformation energy (the energy of the inhibitor components that adjust their shape when adsorbed on the metal), the adsorption energy (the sum of the rigid and deformation energies), and the metal-inhibitor energy (dE_{ads}/d_{Ni}) (the change in adsorption energy when one isoprinosine molecule is removed). The binding energy is the negative value of the adsorption energy. Fig. S3† shows the calculated energies for the inhibitors/Al (1 1 0) surface, including total energy, average total energy, van der Waals energy, electrostatic energy,

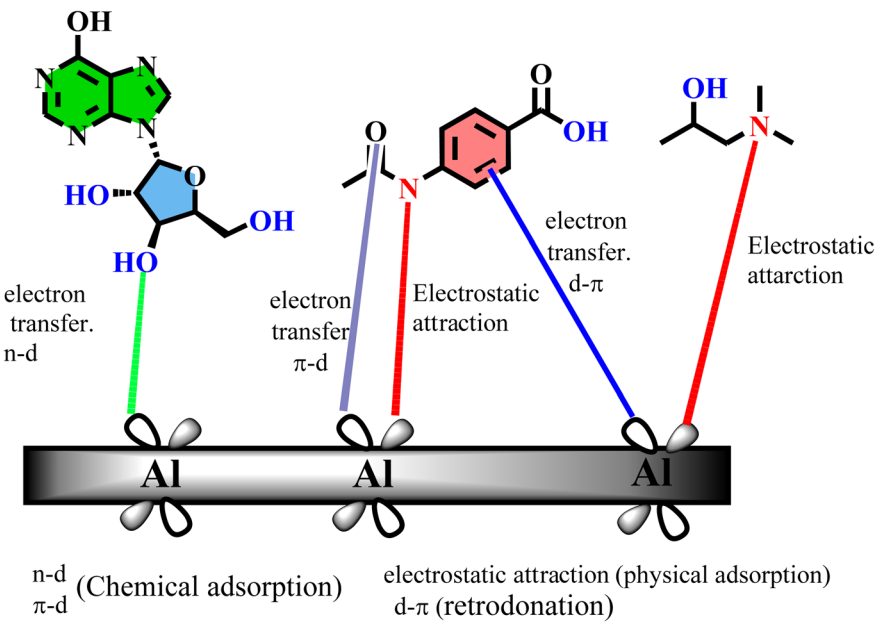

Fig. 10 Mechanism of adsorption of isoprinosine on aluminum surface.

and intramolecular energy. All of the isoprinosine's components displayed coplanar conformation when the structure was stable. Inosine and dimethylaminopropanol were stabilized on the Al (1 1 0) surface in parallel mode, with acedoben placed in perpendicular mode to improve surface contact and protection. Additionally (Table 5), includes a list of the adsorption and binding energies for isoprinosine against the Al (1 0 0) plane. Acedoben > inosine > dimethylaminopropanol are the order of the adsorption energy. The tested inhibitor's N and O lone pairs donate their electrons to the surface of the aluminum atoms' d-orbitales, forming a stable coordination interaction (inhibitor → Al) (Fig. 10). Fig. 10 shows how the C═O and OH groups of isoprinosine can allow for the adsorption of both inhibitors onto the aluminum surface. Consequently, it will prevent an aluminum surface from interacting with the basic solution.

4. Conclusions

Isoprinosine inhibits the corrosion of aluminum, and its impact is concentration-dependent. Isoprinosine adheres to the Langmuir isotherm when adhering to aluminum surfaces in NaOH (0.50 M) solution. Isoprinosine's adsorption on the surface of aluminum causes conduct inhibition, which prevents charge and mass transfer and shields aluminum from corrosive ions. The theoretical calculations agree with the results of the empirical experiments. DFT analysis was utilized to gain a deeper understanding of the electronic structural factors that affect inhibitory efficacy. According to the calculated energy gap, this molecule is stable and has undergone charge transfer. FMO, MEP and Fukui fingerprint are figured, which indicates the charge transfer takes place from isoprinosine to aluminum surface. A molecular dynamic simulation was used to investigate the corrosion inhibition efficiency and the inhibition mechanism.

Institutional review board statement

All procedures were performed in accordance with the Guidelines for Care and Use of Laboratory of Benha University and approved by the Ethics Committee of faculty of science (BUFS-REC-2023-65 chm).

Author contributions

All authors: conceptualization, investigation, methodology, resources, formal analysis, data curation, writing-original draft, writing-review, editing, read & approved the final manuscript.

Conflicts of interest

The authors declare that they have no known competing financial interests or personal relationships that could have appeared to influence the work reported in this paper.

References

1 O. Sanni, A. Popoola, and O. Fayomi, Oil as corrosion inhibitor for aluminium alloy in aggressive environment, in *IOP Conference Series: Materials Science and Engineering*, IOP Publishing, 2018.
2 T. Pesha, *et al.*, Evaluation of corrosion inhibition effect of glycerol stearate on aluminium metal by electrochemical techniques, *Arabian J. Chem.*, 2023, **16**(7), 104798.
3 S. Eid, *et al.*, Corrosion inhibition of aluminum and aluminum silicon alloys in sodium hydroxide solutions by methyl cellulose, *J. Mater. Environ. Sci*, 2015, **6**(3), 892–901.
4 D. Prabhu and P. Rao, Coriandrum sativum L.—A novel green inhibitor for the corrosion inhibition of aluminium in 1.0 M phosphoric acid solution, *J. Environ. Chem. Eng.*, 2013, **1**(4), 676–683.
5 A. Yurt, S. Ulutas and H. Dal, Electrochemical and theoretical investigation on the corrosion of aluminium in acidic solution containing some Schiff bases, *Appl. Surf. Sci.*, 2006, **253**(2), 919–925.
6 H. Ashassi-Sorkhabi, *et al.*, The effect of some Schiff bases on the corrosion of aluminum in hydrochloric acid solution, *Appl. Surf. Sci.*, 2006, **252**(12), 4039–4047.
7 M. Abdallah, *et al.*, Animal glue as green inhibitor for corrosion of aluminum and aluminum-silicon alloys in sodium hydroxide solutions, *J. Mol. Liq.*, 2016, **220**, 755–761.
8 F. V. Adams, *et al.*, Comparison study on the corrosion behavior of aluminum alloys in different acidic media, *Mater. Today: Proc.*, 2021, **38**, 1040–1043.
9 F. T. Owoeye, *et al.*, Investigation of corrosion performance of aluminum and zinc alloys in three acidic media, *Eng. Rep.*, 2020, **2**(1), e12103.
10 M. Abdallah, *et al.*, Gelatin as corrosion inhibitor for aluminum and aluminum silicon alloys in sodium hydroxide solutions, *Prot. Met. Phys. Chem. Surf.*, 2016, **52**, 140–148.
11 M. Lashgari, Theoretical challenges in understanding the inhibition mechanism of aluminum corrosion in basic media in the presence of some p-phenol derivatives, *Electrochim. Acta*, 2011, **56**(9), 3322–3327.
12 A. Abdel-Gaber, *et al.*, Inhibition of aluminium corrosion in alkaline solutions using natural compound, *Mater. Chem. Phys.*, 2008, **109**(2–3), 297–305.
13 J. Ryl, *et al.*, Corrosion inhibition mechanism and efficiency differentiation of dihydroxybenzene isomers towards aluminum alloy 5754 in alkaline media, *Materials*, 2019, **12**(19), 3067.
14 R. Hassan, *et al.*, A revisit to the corrosion inhibition of aluminum in aqueous alkaline solutions by water-soluble alginates and pectates as anionic polyelectrolyte inhibitors, *Int. J. Corros.*, 2013, **2013**, 508596.
15 O. F. Abraham, *et al.*, Corrosion behavior of Aluminium in alkaline-water hyacinth plant extract functionalized solution: An electrochemical and weight loss study, *Chem. Data Collect.*, 2023, **43**, 100983.

16 M. Sobhi and S. Eid, Chemical, electrochemical and morphology studies on methyl hydroxyethyl cellulose as green inhibitor for corrosion of copper in hydrochloric acid solutions, *Prot. Met. Phys. Chem. Surf.*, 2018, **54**, 893–898.
17 S. Eid, Measurement of hydrogen produced during magnesium corrosion in hydrochloric acid and the effect of the triton X-100 surfactant on hydrogen production, *J. Surfactants Deterg.*, 2019, **22**(1), 153–160.
18 S. Eid, *et al.*, Surface, Electrochemical, and Theoretical Investigation on Utilizing Olive Leaf Extract as Green Inhibitor for Copper Corrosion in Alkaline Environment, *Arabian J. Sci. Eng.*, 2023, 1–18.
19 S. Bashir, *et al.*, Corrosion inhibition efficiency of bronopol on aluminium in 0.5 M HCl solution: Insights from experimental and quantum chemical studies, *Surf. Interfaces*, 2020, **20**, 100542.
20 R. K. Hussein, M. Abou-Krisha and T. A. Yousef, Theoretical and experimental studies of different amine compounds as corrosion inhibitors for aluminum in hydrochloric acid, *Biointerface Res. Appl. Chem.*, 2021, **11**(2), 9772.
21 A. Fouda, *et al.*, Tenormin drug as save corrosion inhibitor for 304 stainless steel in hydrochloric acid solutions, *Pharma Chem.*, 2015, **7**(4), 22–33.
22 P. Geethamani, *et al.*, Corrosion inhibition and adsorption properties of mild steel in 1 M hydrochloric acid medium by expired ambroxol drug, *J. Bio- Tribo-Corros*, 2019, **5**, 1–18.
23 S. Eid, Expired desloratidine drug as inhibitor for corrosion of carbon steel pipeline in hydrochloric acid solution, *Int. J. Electrochem. Sci.*, 2021, **16**, 150852.
24 N. A. Khudhair, M. M. Kadhim and A. A. Khadom, Effect of trimethoprim drug dose on corrosion behavior of stainless steel in simulated human body environment: experimental and theoretical investigations, *J. Bio- Tribo-Corros*, 2021, **7**(3), 124.
25 N. O. Eddy, E. E. Ebenso and U. J. Ibok, Adsorption, synergistic inhibitive effect and quantum chemical studies of ampicillin (AMP) and halides for the corrosion of mild steel in H 2 SO 4, *J. Appl. Electrochem.*, 2010, **40**, 445–456.
26 R. Ganapathi Sundaram, G. Vengatesh and M. Sundaravadivelu, Adsorption behavior and anticorrosion capability of antibiotic drug nitroxoline on copper in nitric acid medium, *J. Bio- Tribo-Corros*, 2017, **3**, 1–13.
27 N. J. Maduelosi and N. B. Iroha, Insight into the adsorption and inhibitive effect of spironolactone drug on C38 carbon steel corrosion in hydrochloric acid environment, *J. Bio-Tribo-Corros*, 2021, **7**(1), 6.
28 I. Akande, O. Fayomi and O. Oluwole, Anticorrosion potential of inhibitive suphtrim drug on aluminium alloys in 0.5 MH 2 SO 4, *J. Bio- Tribo-Corros*, 2020, **6**, 1–8.
29 N. Vaszilcsin, V. Ordodi and A. Borza, Corrosion inhibitors from expired drugs, *Int. J. Pharm.*, 2012, **431**(1–2), 241–244.
30 P. Su, *et al.*, Expired drug theophylline as potential corrosion inhibitor for 7075 aluminium alloy in 1M NaOH solution, *Int. J. Electrochem. Sci.*, 2020, **15**(2), 1412–1425.
31 M. Lavanya, J. Ghosal and P. Rao, A comprehensive review of corrosion inhibition of aluminium alloys by green inhibitors, *Can. Metall. Q.*, 2024, **63**(1), 119–129.
32 H. M. K. Sheit, *et al.*, Experimental Studies on the Effect of Expired Amiodarone Drug (EAD) as a Corrosion Inhibitor on Mild Steel in 1 M HCl, *Materials*, 2024, **17**(3), 751.
33 M. A. Ibrahim, *et al.*, Density functional theory study of the corrosion inhibition performance of 6-mercaptopurine and 6-thioguanine expired drugs toward the aluminium (111) surface, *RSC Adv.*, 2023, **13**(41), 29023–29034.
34 A. Al Bahir, Evaluation of expired linezolid and norfloxacin drugs as proficient environmentally safe inhibitors for mitigation of aluminum corrosion in sodium chloride medium, *Chem. Data Collect.*, 2022, **42**, 100960.
35 M. M. Motawea and S. Melhi, Electrochemical and computational studies of an expired vilazodone Drug as environmentally safe corrosion inhibitor for aluminum in chloride medium, *J. Indian Chem. Soc.*, 2023, **100**(6), 101013.
36 M. Abdallah, *et al.*, Enhancing the inhibition and adsorption performance of SABIC iron corrosion in sulfuric acid by expired vitamins. Experimental and computational approach, *RSC Adv.*, 2021, **11**(28), 17092–17107.
37 H. A. Mohamedien, *et al.*, Experimental and computational evaluations of cefotaxime sodium drug as an efficient and green corrosion inhibitor for aluminum in NaOH solution, *Mater. Chem. Phys.*, 2022, **290**, 126546.
38 M. Quraishi and D. S. Chauhan, Recent trends in the development of corrosion inhibitors, in *A Treatise on Corrosion Science, Engineering and Technology*, Springer, 2022, pp. 783–799.
39 C. Verma, *et al.*, Recent developments in sustainable corrosion inhibitors: design, performance and industrial scale applications, *Mater. Adv.*, 2021, **2**(12), 3806–3850.
40 R. A. Hameed, *et al.*, Expired Voltaren drugs as corrosion inhibitor for aluminium in hydrochloric acid, *Int. J. Electrochem. Sci.*, 2015, **10**(3), 2098–2109.
41 R. Nathiya, *et al.*, Expired drugs: environmentally safe inhibitors for aluminium corrosion in 1 MH 2 SO 4, *J. Bio-Tribo-Corros*, 2018, **4**, 1–13.
42 H. A. Mohamedien, *et al.*, Electrochemical and computational estimations of cephalosporin drugs as eco-friendly and efficient corrosion inhibitors for aluminum in alkaline solution, *Sci. Rep.*, 2022, **12**(1), 13333.
43 M. Abdallah, *et al.*, Sildenafil drug as a safe anticorrosion for 6063 aluminum alloy in acidic and alkaline solutions: Theoretical and experimental studies, *Egypt. J. Pet.*, 2020, **29**(3), 211–218.
44 M. Abdallah, *et al.*, Inhibitive performance of dapoxetine drug for corrosion of aluminum alloy (AA6063) in acidic and alkaline solutions: experimental and theoretical studies using Materials Studio v7. 0, *Desalin. Water Treat.*, 2021, **221**, 270–280.
45 S. Sharma, *et al.*, Overview of BIOVIA Materials Studio, LAMMPS, and GROMACS, *Molecular Dynamics Simulation of Nanocomposites Using BIOVIA Materials Studio, LAMMPS and GROMACS*, Elsevier, Amsterdam, The Netherlands, 2019.

46 V. A. Basiuk and L. V. Henao-Holguín, Dispersion-corrected density functional theory calculations of meso-tetraphenylporphine-C60 complex by using DMol3 module, *J. Comput. Theor. Nanosci.*, 2014, **11**(7), 1609–1615.
47 P. Kwolek, *et al.*, Gallic acid as a potential green corrosion inhibitor for aluminum in acidic solution, *Metals*, 2022, **12**(2), 250.
48 R. Norsworthy, Understanding corrosion in underground pipelines: basic principles, in *Underground Pipeline Corrosion*, Elsevier, 2014, pp. 3–34.
49 R. K. Gupta, *et al.*, Aminoazobenzene and diaminoazobenzene functionalized graphene oxides as novel class of corrosion inhibitors for mild steel: experimental and DFT studies, *Mater. Chem. Phys.*, 2017, **198**, 360–373.
50 I. Akande, O. Oluwole and O. Fayomi, Optimizing the defensive characteristics of mild steel via the electrodeposition of ZnSi3N4 reinforcing particles, *Def. Technol.*, 2019, **15**(4), 526–532.
51 O. K. Abiola and J. Otaigbe, Effect of common water contaminants on the corrosion of aluminium alloys in ethylene glycol–water solution, *Corros. Sci.*, 2008, **50**(1), 242–247.
52 D. F. Seyam, *et al.*, Study of the inhibition effect of two novel synthesized amido-amine-based cationic surfactants on aluminum corrosion in 0.5 M HCl solution, *J. Surfactants Deterg.*, 2022, **25**(1), 133–143.
53 A. A. Khadom and A. S. Yaro, Mass transfer effect on corrosion inhibition process of copper–nickel alloy in hydrochloric acid by Benzotriazole, *J. Saudi Chem. Soc.*, 2014, **18**(3), 214–219.
54 N. Al Otaibi and H. H. Hammud, Corrosion inhibition using harmal leaf extract as an eco-friendly corrosion inhibitor, *Molecules*, 2021, **26**(22), 7024.
55 C. Verma, *et al.*, Electrochemical, thermodynamic, surface and theoretical investigation of 2-aminobenzene-1, 3-dicarbonitriles as green corrosion inhibitor for aluminum in 0.5 M NaOH, *J. Mol. Liq.*, 2015, **209**, 767–778.
56 R. Padash, *et al.*, Corrosion control of aluminum in the solutions of NaCl, HCl and NaOH using 2, 6-dimethylpyridine inhibitor: Experimental and DFT insights, *Mater. Chem. Phys.*, 2020, **244**, 122681.
57 A. Abdel-Gaber, *et al.*, Novel package for inhibition of aluminium corrosion in alkaline solutions, *Mater. Chem. Phys.*, 2010, **124**(1), 773–779.
58 Z. Moghadam, M. Shabani-Nooshabadi and M. Behpour, Electrochemical performance of aluminium alloy in strong alkaline media by urea and thiourea as inhibitor for aluminium-air batteries, *J. Mol. Liq.*, 2017, **242**, 971–978.
59 M. A. Amin, *et al.*, Polyacrylic acid as a corrosion inhibitor for aluminium in weakly alkaline solutions. Part I: Weight loss, polarization, impedance EFM and EDX studies, *Corros. Sci.*, 2009, **51**(3), 658–667.
60 D. D. Macdonald, Review of mechanistic analysis by electrochemical impedance spectroscopy, *Electrochim. Acta*, 1990, **35**(10), 1509–1525.
61 A. Singh, I. Ahamad and M. A. Quraishi, Piper longum extract as green corrosion inhibitor for aluminium in NaOH solution, *Arabian J. Chem.*, 2016, **9**, S1584–S1589.
62 N. Chaubey, *et al.*, A comparative study of leaves extracts for corrosion inhibition effect on aluminium alloy in alkaline medium, *Ain Shams Eng. J.*, 2017, **8**(4), 673–682.
63 D. K. Yadav and M. Quraishi, Electrochemical investigation of substituted pyranopyrazoles adsorption on mild steel in acid solution, *Ind. Eng. Chem. Res.*, 2012, **51**(24), 8194–8210.
64 M. A. Abbas, *et al.*, Performance assessment by experimental and Theoretical approaches of newly synthetized benzyl amide derivatives as corrosion inhibitors for carbon steel in 1.0 M hydrochloric acid environment, *Inorg. Chem. Commun.*, 2022, **143**, 109758.
65 M. Bedair, *et al.*, Benzidine-based Schiff base compounds for employing as corrosion inhibitors for carbon steel in 1.0 M HCl aqueous media by chemical, electrochemical and computational methods, *J. Mol. Liq.*, 2020, **317**, 114015.
66 A. H. Ahmed, *et al.*, Ethanedihydrazide as a corrosion inhibitor for iron in 3.5% NaCl solutions, *ACS Omega*, 2021, **6**(22), 14525–14532.
67 N. H. Alharthi, *et al.*, Corrosion inhibition of mild steel by highly stable polydentate schiff base derived from 1, 3-propanediamine in aqueous acidic solution, *J. Saudi Chem. Soc.*, 2022, **26**(4), 101501.
68 S. Eid, *et al.*, Combination of Experimental and Computational Insight into the Anti-corrosion Performance of 1-(4-tert-butylphenyl)-4-(4-(benzhydryloxy) piperidin-1-yl) butan-1-one onto C-steel in Acidic Environments, *J. Bio- Tribo-Corros*, 2023, **9**(3), 61.
69 S. Syam, *et al.*, Combination of practical and theoretical measurements of albumin egg as an eco-friendly inhibitor for copper corrosion in alkaline solutions, *RSC Adv.*, 2023, **13**(48), 33929–33942.
70 M. M. Khowdiary, *et al.*, Synthesis of novel nano-sulfonamide metal-based corrosion inhibitor surfactants, *Materials*, 2022, **15**(3), 1146.
71 H. Laaroussi, *et al.*, Experimental and Theoretical Investigations of Argania spinosa's Extracts on the Antioxidant Activity and Mild Steel Corrosion's Inhibition in 1 M HCl, *Appl. Sci.*, 2022, **12**(24), 12641.
72 P. Vinet, T. Lemogne and H. Montes, *Aluminum Work Function: Effect of Oxidation, Mechanical Scraping and Ion Bombardment*, 1985.
73 M. H. Alsehli, *et al.*, Synthesis, Cytotoxic Activity, Crystal Structure, DFT, Molecular Docking Study of β-Enaminonitrile Incorporating 1 H-Benzo [f] Chromene Moiety, *Crystals*, 2022, **13**(1), 24.
74 M.-Y. Hjouji, *et al.*, Exploring Antimicrobial Features for New Imidazo [4, 5-b] pyridine Derivatives Based on Experimental and Theoretical Study, *Molecules*, 2023, **28**(7), 3197.